Heterogeneous catalytic properties of unprecedented μ-O-[FeTCPP]$_2$ dimers (H_2TCPP = *meso*-tetra(4-carboxyphenyl)porphyrin): unusual superhyperfine EPR structure

Arkaitz Fidalgo-Marijuan,[a] Gotzone Barandika,*[b] Begoña Bazán,[a,d] Miren Karmele Urtiaga,[a] Edurne S. Larrea,[a] Marta Iglesias,[c] Luis Lezama[b,d] and María Isabel Arriortua[a,d]

Received (in XXX, XXX) Xth XXXXXXXXX 20XX, Accepted Xth XXXXXXXXX 20XX
DOI: 10.1039/b000000x

During the past years, a great effort has been devoted to the anchoring of catalysts into solid coordination networks in order to achieve heterogeneous catalysts. In this sense, an innovative approach consists on using the coordination-network synthons both as structural units and as catalysts. Regarding the latter, metalloporphyrins are suitable candidates for synthons. In fact, a few works report on coordination compounds based on metalloporphyrins exhibiting these features. On the other hand, highly distorted di-iron oxo dimers containing electron withdrawing groups rank amongst the most-effective catalyst models. Thus, the aim of this work was obtaining coordination networks based on iron porphyrins exhibiting those characteristics. This way, this work reports on the synthesis and characterisation of the μ-O-[FeTCPP]$_2$·16DMF compound (H_2TCPP = *meso*-tetra(4-carboxyphenyl)porphyrin, DMF = N,N-dimethylformamide). This compound is the first example of an μ-oxo dimer with TCPP. The inter-dimer connections give rise to a laminar structure. The structural, spectroscopic and magnetic properties of this compound are consistent with the presence of high-spin Fe^{III} ions, exhibiting a strong antiferromagnetic coupling in the μ-oxo dimer (J = -132 cm^{-1}). An unusual superhyperfine structure has been observed in EPR that is related to the high accessible volume of the compound. The structural features of the dimers and the accessible network are responsible for the excellent behaviour of the compound as a heterogeneous catalyst for different oxidation of alcohols. Therefore, this compound is a new of the very few examples of metalloporphyrins where structural units play as catalysts.

Introduction

Solid coordination networks consist of metal complexes that can be packed in a variety of frameworks.[1-3] They have been thoroughly explored in many fields, such as gas storage and separation,[4,5] nonlinear optics,[6,7] ferroelectricity,[8] conductivity,[9] magnetism,[10] luminescence,[11] biomedical imaging,[12] chemical sensing,[13] drug delivery[14] and heterogeneous catalysis.[15-17] Among the different organic ligands that can be used in these coordination networks, metalloporphyrins can be highlighted as they can produce unique properties attached to biochemical, enzymatic and photochemical functions.[18] Thus, an efficient synthesis strategy can give rise to compounds capable to mimic these properties.

Biomimetic catalysts such as metalloporphyrins have been used as cytochrome P-450 models, and their potential for substrate oxidation has been the subject of several studies.[19-21] The similarity between metalloporphyrins and the active centre of many natural enzymes, along with the high reactivity and selectivity towards oxidation of organic substrates, have stimulated the use of iron porphyrins as models of natural catalysts.[22] In this sense, a large number of model systems have been explored,[23-26] and the use of highly distorted di-iron oxo dimers containing electron withdrawing groups rank amongst the most-effective catalyst models attracting considerable attention on the last years.[27-29] Some μ-oxo dimers of FeTPP (TPP= *meso*-tetra(4-phenyl)porphine) have been used as model compounds of cytochromes P-450, and they exhibit greater catalytic activity than the FeTPP monomers.[30]

In order to achieve heterogeneous catalysts, there are successful approaches consisting of anchoring the catalyst into the cavities of porous coordination networks,[31-33] doping the network with the catalyst[34] or post functionalizing the network.[35,36] Thus, our proposal is using the catalyst as a structural unit. As concluded by several recent works,[37-49] this approach has been observed to be effective. However, the number of metalloporphyrinic compounds in which the network itself plays as a catalyst is very low.

In this sense, our previous research on metalloporphyrins[50-53] has had the same goal. However, we have not been successful until now. The selection of H_2TCPP (H_2TCPP = *meso*-tetra(4-carboxyphenyl)porphine) must be underlined in this sense

(Scheme 1).

There are some TCPP-based coordination compounds in literature, and they exhibit different types of packing.[50,54,55] On the other hand, most of the reported μ-oxo dimers are of the FeTPP type[56-63] (H_2TPP = *meso*-tetra(4-phenyl)porphyrin, or octaethylporphyrins (OEP).[28,64-77] However, as far as we are concerned, no dimers of the μ-oxo FeTCPP-type have been reported so far.

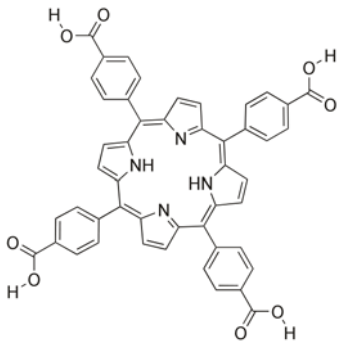

Scheme 1 Lewis structure for H_2TCPP (hydrogen atoms in the H_2TCPP acronym correspond to the pyrrole nitrogen atoms).

Taking into account the above mentioned aspects, this work reports on the first TCPP based μ-oxo dimer with formula μ-O-[FeTCPP]$_2$·16DMF (DMF = N,N-dimethylformamide). Hydrogen bonds produce a 2D array, and interlayer π-π interactions give rise to the 3D network. The compound has been exhaustively characterised by means of X-ray diffraction, IR, Raman, UV-Vis, Mössbauer and EPR (Electron Paramagnetic Resonance) spectroscopies, thermogravimetric analysis, magnetic susceptibility measurements and catalytic activity tests. Distortion of the porphyrin macrocycle has also been analysed.

Experimental section

Materials

All solvents and chemicals were used as received from reliable commercial sources. The reagent iron (III) *meso*-tetra(4-carboxyphenyl)porphyrin chloride ([FeTCPP]Cl) was purchased from Frontier Scientific, and isophthalic acid (99%) and the solvent N,N-dimethylformamide (DMF, 99.8%) were purchased from Sigma-Aldrich Co.

X-ray structure determination

Prismatic black single-crystals of μ-O-[FeTCPP]$_2$·16DMF with dimensions given in Table 1 were selected under polarizing microscope and mounted on MicroMounts™. Single-crystal X-ray diffraction data were collected at 100 K on an Agilent Technologies SuperNova single source diffractometer with Cu-Kα radiation (λ=1.54184 Å). Data frames were processed (unit cell determination, intensity data integration, correction for Lorentz and polarization effects,[78] and analytical absorption correction) using the CrysAlis software package.[79] The structure of μ-O-[FeTCPP]$_2$·16DMF was solved in the monoclinic *C*2/c space group with Superflip program,[80] which allowed us to obtain the position of iron atom, as well as nitrogen, oxygen and some of the carbon atoms of the TCPP anion. The refinement of the crystal structure was performed by full matrix least-squares based on F^2, using the SHELXL-97 program[81] in OLEX[82] obtaining the remaining carbon atoms. Anisotropic thermal parameters were used for all non-hydrogen atoms (Figure S1, ESI†). All the hydrogen atoms connected to the aromatic rings (C-H 0.95Å) were fixed geometrically, and were refined using a riding model with common isotropic displacements. The hydrogen atoms of the carboxylic groups were not considered due to the lack of density in the residual density map; however they are included in the formula. DMF molecules were disordered in the crystal and the resulting electron density was found to be non interpretable. The solvent contribution to the structure factors was taken into account by back-Fourier transformation of all density found in the disordered area using a solvent mask in OLEX.[82] The calculated density does not take account of the solvent. Bond distances and angles, atomic coordinates, anisotropic thermal parameters and hydrogen atom coordinates are given in Tables S1, S2, S3 and S4, ESI†.

From a crystallographic point, compound μ-O-[FeTCPP]$_2$·16DMF can be described by using Z=8, in accordance with the space group and the asymmetric unit. However, Z=4 has been selected because this way the whole dimer is represented in the chemical formula.

Table 1 Crystallographic data for μ-O-[FeTCPP]$_2$·16DMF.

Compound	μ-O-[FeTCPP]$_2$·16DMF
Formula	$C_{144}H_{168}Fe_2N_{24}O_{33}$
FW, g·mol^{-1}	2874.71
Crystal system	Monoclinic
Space group (no. 15)	*C*2/c
a, Å	39.3340(4)
b, Å	19.8329(2)
c, Å	16.0292(2)
β, deg	98.4180(10)
V, Å ^{3}	12369.8(2)
Z	4
ρ_{obs}, ρ_{cal}, g·cm^{-3}	1.575(5), 0.911
F(000)	3472
μ, mm^{-1}	2.304
Crystal size, mm	0.21 x 0.12 x 0.05
Absorption correction	Analytical
Radiation, λ, Å	1.54184
Temperature, K	100(2)
Reflections collected, unique	50744, 12049 (R_{int}=0.04)
Limiting indices	-48<=*h*<=47
	0<=*k*<=24
	0<=*l*<=19
Refinement method	Full-matrix least-squares on F^2
Final *R* indices [I > 2σ(I)][a]	R1 = 0.0608, wR2 = 0.1867
R indices (all data)[a]	R1 = 0.0788, wR2 = 0.2025
Goodness of fit on F^2	1.063
Parameters /restraints	555 / 0

[a]$R1=[(|F_0|- |F_c|)]/|F_0|$. $wR2=[[w|F_0|^2-|F_c|^2)^2]/[w(|F_0|^2)^2]^{1/2}$

Physicochemical characterisation techniques

The IR spectra were collected on a JASCO FT/IR-6100 spectrometer at room temperature at the range of 4000-400 cm^{-1}, in KBr pellets (1% of the sample). Raman spectra of the solid samples were recorded using a Renishaw InVia spectrometer equipped with a 785 nm laser at the range of 3500-150 cm^{-1}. UV-visible diffuse-reflectance measurements were carried out on a Cary 5000 UV-Vis-NIR spectrophotometer in the range of 2500

to 200 nm. C, H, N and O elemental analyses were measured using a Euro EA 3000 elemental analyser. The thermal analyses were carried out in air atmosphere using a NETZSCH STA 449F3 instrument. A crucible containing approximately 10 mg of sample was heated at 5 ºC min^{-1} in the temperature range 30-600 ºC. Mössbauer spectra were obtained at room temperature using a constant-acceleration Mössbauer spectrometer with a $^{57}Co/Rh$ source. The velocity calibration was done using a metallic Fe foil. Electron paramagnetic resonance (EPR) spectra were measured with a Bruker ESP-300 spectrometer operating at X band and equipped with a nitrogen and helium cryostat. Magnetic susceptibility measurements were measured in the range of 4−300 K with a Quantum Design SQUID MPMS-7T magnetometer.

Catalytic Tests

The oxidation reactions of benzyl alcohol, 1-phenylethanol, 1-hexanol and 1-octanol (Scheme 2) were carried out at 70 ºC using acetonitrile as solvent. The catalyst/substrate molar ratio (based on Fe) used for all the reactions is 3 %.

Powdered crystals of catalyst was firstly dried at 100 ºC and under vacuum to remove solvent and water adsorbed at the surface. Before the reactions, approximately 5 mg of dried catalyst (0.0035 mmol of Fe) were activated by stirring it with the oxidizing agent, *tert*-butyl hydroperoxide (TBHP) or iodobenzene diacetate ($PhI(OAc)_2$), in 2 ml of acetonitrile, for 30 min at 70 ºC. After this activation stage, the catalyst was separated from the liquid media by centrifugation. The reactor was then charged with the activated catalyst, 0.12 mmol of the corresponding alcohol in 2 mL of solvent. The mixture was heated up to 70 ºC and then the oxidizing agent was added dropwise (1.5 eq. in the case of TBHP and 2 eq. in the case of $PhI(OAc)_2$). All the data corresponding to the different reactions made for this study are summarized in table S5, ESI†.

Reaction samples were taken at regular times and analysed on a Hewlett–Packard 5890 II GC-MS gas chromatograph-mass spectrometer. Blank experiments were carried out under the reaction conditions in order to determine the extension of the uncatalysed reaction, and only traces of products were achieved after 7 h.

After the reaction, the catalysts were filtered and characterised by IR spectroscopy. Due to the low crystallinity of μ-O-$[FeTCPP]_2$·16DMF, X-ray powder diffraction was rejected as a characterisation technique for the recovered catalyst.

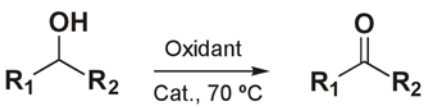

Scheme 2 Catalytic tests reaction.

The calculations of turnover numbers (TON: mol subs. conv./mol cat.) were made with respect to the iron amount, assuming that the metal centre is the active species in the catalyst. Turnover frequencies (TOF) were calculated in the initial stages of the reaction, when the reaction rates are higher, as usual.

Results and Discussion

Synthesis of μ-O-$[FeTCPP]_2$·16DMF

Iron (III) *meso*-tetra(4-carboxyphenyl)porphine chloride (8.8 mg, 0.01 mmol) and isophthalic acid (9.9 mg, 0.06 mmol) were dissolved in DMF (4 mL) in a small capped vial, sonicated to ensure homogeneity and heated to 80 ºC for 72 h, following by slow cooling to room temperature, yielding diffraction quality prismatic black crystals. (Yield: 36%, Found: C, 66.91; H, 3.17; N, 6.54; O, 16.40. Calc. for $C_{96}H_{56}Fe_2N_8O_{17}$: C, 67.62; H, 3.31; N, 6.57; O, 15.95).

Crystal structure

Crystal structure of μ-O-$[FeTCPP]_2$·16DMF was determined by means of X-ray single crystal diffraction. The structure shows that two FeTCPP rings are bonded together by a bridging O atom in a Fe-O-Fe bond system (Figure 1a). TCPP anions are divalent (hydrogen atoms in H_2TCPP acronym correspond to the pyrrole nitrogen atoms). The iron atom is on a five-coordinated square pyramidal environment, displaced by 0.445 Å from the mean porphyrin plane (24 atoms) towards the oxo-bridge, and forms a nearly lineal Fe-O-Fe angle (179.78º). The Fe-N_p distances are in the narrow range of 2.077(2) to 2.087(2) Å, while the Fe-O distance is 1.7597(4) Å. These distances and angles are typical for high-spin iron (III) μ-oxo dimers.[28,30,56-59,64,69,83-87] The macrocyclic rings are essentially parallel to each other, the angle between the two central N_4 planes being 0.31º. The relative orientations of the two porphyrin rings make an average N_p-Fe-Fe´-N´$_p$ dihedral angle (torsional angle) of 33.62º (Figure 1b) to accommodate the peripheral carboxylic groups (N_p accounts for the pyrrolic nitrogen atoms).

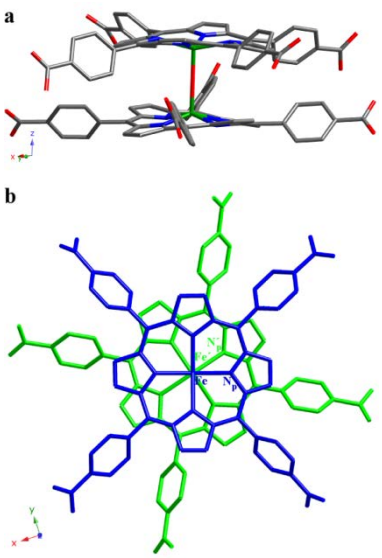

Fig. 1 (a) Dimeric unit for μ-O-$[FeTCPP]_2$·16DMF. Colour code: Fe= Green, N= Blue, C= Grey and O= red. H atoms have been omitted for clarity and (b) top view of the dimer.

These coordination entities crystallise as shown in Figure 2. Each dimer is surrounded by another six producing an H-bonded 2D layer on the *xy* plane. The robust intralayer H-bonding system is generated from O8 to O4 (2.411 Å) and from O7 to O2 (2.470 Å) maintaining the stability of the layers.

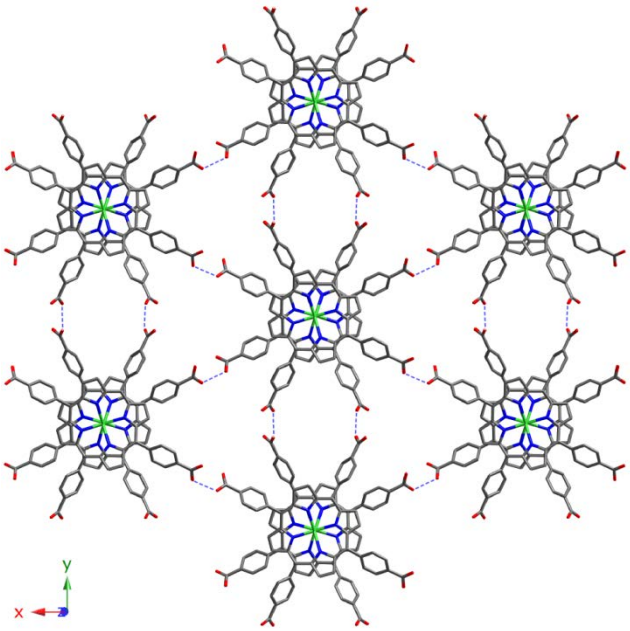

Fig. 2 View of the H-bonded 2D layer for μ-O-[FeTCPP]$_2$·16DMF. Colour code: Fe= Green, N= Blue, C= Grey, O= red and H-bonds= Dashed lines. H atoms have been omitted for clarity.

The H-bonded 2D layers are stacked along the (001) direction, sustained by π-π interactions (3.5~3.9 Å) among the dimers of each layer (Figure 3). Crystallisation DMF molecules are located in the voids generated between dimers. Unfortunately, these molecules have not been located in the structure refinement process. The resulting solvent accessible volume, removing the DMF molecules, was analysed with PLATON program,[88] showing a potential solvent volume of 5836.2 Å^3 (47.2% of the unit cell) and a calculated effective volume of 2470.1 Å^3. Taking into account the single crystal experimental density, the initial weight loss observed in the thermogravimetric analysis and the calculated free effective volume, we have estimated the presence of 16 DMF molecules per formula unit. These DMF molecules should be located on the two types of voids in the crystal structure (along the *c* axis and interweaving the 2D layers).

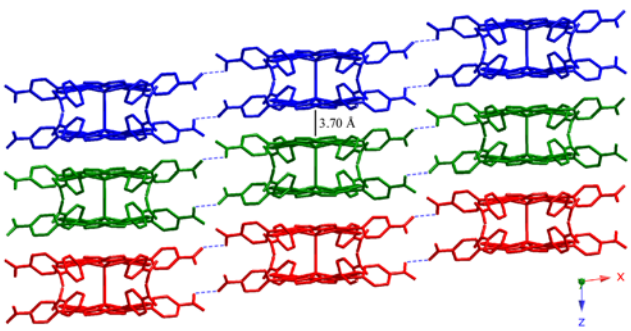

Fig. 3 Stacking of the 2D layers for μ-O-[FeTCPP]$_2$·16DMF, where each layer is shown in a different colour. Intralayer H-bonds are shown as dashed lines. H atoms have been omitted for clarity.

The out-of-plane distortion of the porphyrin macrocycle was analysed by the normal-coordinate structural decomposition method developed by Shelnutt *et al.* (NSD).[89,90] In a saddle conformation, alternate pyrrole rings tilt up and down with respect to the porphyrin mean plane (24 atoms), and the *meso* carbon atoms lie on the least-square plane. As is evident from Figure 4, the results indicate a main saddle type distortion (*sad*, B_{2u}), with a contribution of the 82% to the total displacement of the porphyrin (1.502).

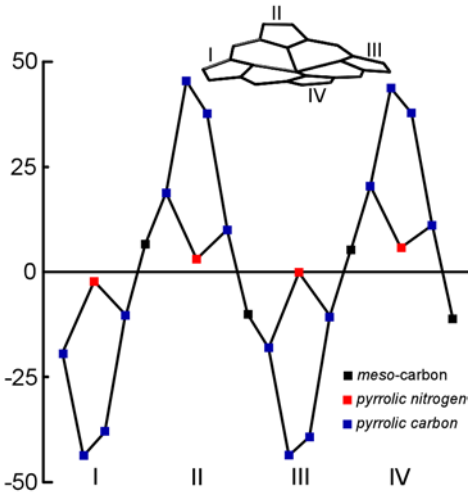

Fig. 4 Out-of-plane displacements (in units of 0.01 Å) of the porphyrin core atoms from the mean porphyrin plane (of 24 atom) for μ-O-[FeTCPP]$_2$·16DMF.

This nonplanarity of the porphyrin core is the consequence of significant steric congestion in the periphery of the molecule. The slight saddle distortion on the two porphyrin cores and the value of the Fe atom displacement from the mean porphyrin plane (0.445 Å) is consistent with the presence of high spin (S=5/2) Fe^{III} ions.[76,91] This fact, as will be seen later, was corroborated by EPR and Mössbauer spectroscopies and by magnetic measurements.

Infrared and Raman spectroscopies

The most significant IR spectral changes from the reactant [FeTCPP]Cl porphyrin to the final dimer account for the formation of the μ-oxo diiron(III) bond, with the appearance of two new strong absorptions at 870 and 827 cm^{-1}. It is well known that the antisymmetric stretching mode (ν_3), specifically the ν_{as}(Fe-O-Fe), of a linear or bent Fe-O-Fe system usually occurs in the range 900-800 cm^{-1}.[92] Thus, these two absorptions, at 870 and 827 cm^{-1}, indicate the presence of a Fe-O-Fe bond. The rest of the observed absorptions are the usual ones for porphyrin compounds: ν_{max}/cm^{-1} 3414 and 1433 (OH), 3031 (C(sp^2)H), 1705 and 1202 (CO), 1632 (DMF), 1606-1476 (CC), 1383 (CN), 999 (FeTCPP) (Figure S2, ESI†).

While for IR spectra the dominant feature is the antisymmetric Fe-O-Fe absorption, Raman spectra are expected to show a greater contribution of the symmetric Fe-O-Fe vibration. Previous works[83,93] have identified that the vibrations around 363 cm^{-1} in Raman spectra correspond to the out-of-plane symmetric Fe-O-Fe stretching mode. Thus, μ-O-[FeTCPP]$_2$·16DMF shows Raman spectral band at 363.3 cm^{-1}, which is identified as the ν_{as}(Fe-O-Fe) mode. Furthermore, the additional bands observed in the Raman spectra are mainly porphyrin skeletal vibration modes, including $\nu_{as}(C_\alpha C_m)$ (1608), $\nu(C_\beta C_\beta)$ (1550), ν_s(pyrrole half-ring) (1360), $\delta(C_m H)$ (1233) and δ_{as}(pyrrole deform) (991) (Figure S3, ESI†).

UV-Visible (Diffuse-Reflectance) spectroscopy

The UV-Vis spectrum of μ-O-[FeTCPP]$_2$·16DMF shows Soret and Q bands at 361, 576 and 623 nm, respectively (Figure S4, ESI†). The evident blueshift of the Soret band, compared to other iron (III) non-dimeric porphyrin compounds and to the monomeric [FeTCPP],[94] reflects the short interporphyrin ring separation, whereas the Q bands are redshifted by the presence of carboxylic groups on the periphery of the porphyrin.

Thermogravimetry

The thermogravimetric decomposition curve of the compound shows an initial two-stage mass loss from RT to 360 ºC, assigned to the removal of DMF molecules (40.95% weight loss) from the two types of voids in the crystal structure. Afterwards, a second mass loss occurs from 360 ºC to 400 ºC, assigned to both porphyrin units (51.5% weight loss) (Figure S5, ESI†). The calcination product has been identified by powder X-ray diffraction analysis, and it consists of Fe_2O_3 [space group *R*-3*c*, *a* = 5.0142 Å, *c* = 13.6733 Å and γ = 120º].[95]

Mossbauer spectroscopy

Compound μ-O-[FeTCPP]$_2$·16DMF has been studied by Mössbauer spectroscopy. The spectrum has been simulated with the NORMOS program,[96] and indicates the presence of a doublet corresponding to Fe^{III} signals. The signal is assigned to the metal ions in μ-O-[FeTCPP]$_2$·16DMF. The isomer shift (δ) and quadrupolar splitting (ΔE) values are 0.270(6) and 0.623(9), respectively, in the range usually observed for high spin Fe^{III} porphyrins[76] (Figure 5).

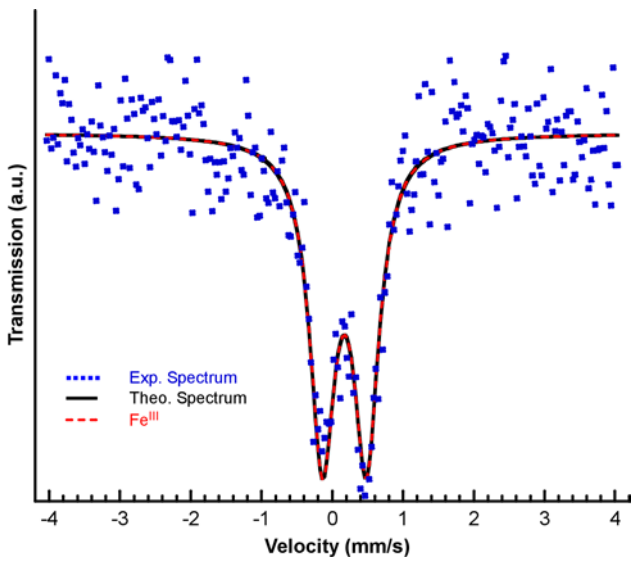

Fig. 5 Mössbauer spectra for μ-O-[FeTCPP]$_2$·16DMF.

Magnetic measurements

Variable temperature magnetic susceptibility measurements have been carried out between 5 and 300 K for μ-O-[FeTCPP]$_2$·16DMF, and the plot of $\chi_m T$ versus T is shown in Figure 6. The effective magnetic moment decreases from 4.43 μ_B at 300 K to 4.03 μ_B at 75 K. After a slow decrease, down to 15 K, the effective magnetic moment suffers another abrupt decrease, reaching the value of 3.47 μ_B at 5 K.

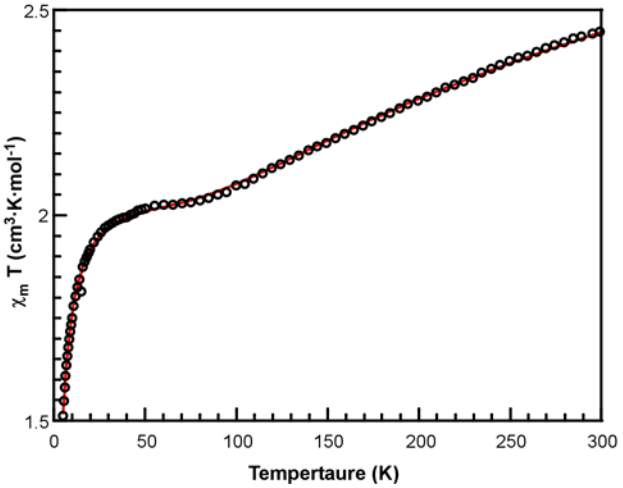

Fig. 6 Thermal evolution of the $\chi_m T$ product for μ-O-[FeTCPP]$_2$·16DMF compound.

The high-temperature behaviour is the expected for a strong antiferromagnetic coupling in a S = 5/2 dimer. However, the plateau between 75 and 15 K, and the further abrupt decrease cannot be explained by the sole contribution of this coupling. X-ray analysis discards the presence of impurities in the required high concentration as to account for the observed curve. However, we can think of the presence of broken dimers that are expected to be paramagnetic. The dimers are expected to be broken because the magnetic measurements were performed by using ground single crystals, producing monomeric units. Thus, the decrease in the effective magnetic moment observed at low temperatures can be explained by means of the Zero Field Splitting effect (ZFS) on the S = 5/2 state.

In order to confirm this hypothesis, experimental data have been adjusted according to equation 1 where χ_{dim} and χ_{mon} are the contribution of the dimeric and monomeric (broken dimers) species, respectively.

$$\chi_m = (1-\delta)\,\chi_{dim} + \delta\,\chi_{mon} \qquad (1)$$

In order to evaluate the exchange constant J due to the contribution of the dimeric species (χ_{dim}), the van Vleck equation has been used for a spin Hamiltonian H=-2JS_1S_2 (equation 2).

$$\chi_m = \frac{2Ng^2\beta^2}{kT}\,\frac{exp(2x)+5\,exp(6x)+14\,exp(12x)+30\,exp(20x)+55\,exp(30x)}{1+3\,exp(2x)+5\,exp(6x)+7\,exp(12x)+9\,exp(20x)+11\,exp(30x)}$$

where x=J/kT (2)

The van Vleck equation has been also used to estimate the exchange constant J due to the contribution of the monomeric species (χ_{mon}), but in this case for S = 1/2 in an axially distorted octahedral environment (equation 3). In equation 3, D is the axial parameter related to the ZFS effect, The E rhombic one has been considered negligible.

$$\chi_{\parallel} = \frac{Ng^2_{\parallel}\beta^2}{4kT}\,\frac{1+9\,exp(-2x)+25\,exp(-6x)}{1+exp(-2x)+exp(-6x)}$$

$$\chi_{\perp} = \frac{Ng^2_{\perp}\beta^2}{4kT}\,\frac{9+8/x-11\,exp(-2x)/2x-5\,exp(-6x)/2x}{1+exp(-2x)+exp(-6x)}$$

where x=D/kT (3)

Taking into account that the orbital contribution for S = 5/2 ions is habitually negligible, the g value was considered to be g=2. This way, the number of parameters to be adjusted was lower, producing estimated values of J = -132 cm^{-1}; D = 6.9 cm^{-1} and δ= 0.23. These values were obtained by minimizing the R error (equation 4). Figure 6 shows that experimental and calculated values are in very good accordance ($R=1.2x10^{-5}$). The J value is comparable to other ones found for similar systems.[63,69,97] It is worth mentioning that the δ value indicates a significant amount of monomeric species.

$$R=\Sigma[\chi_m T^{exp} - \chi_m T^{cal}]^2 / \Sigma[\chi_m T^{exp}]^2 \quad (4)$$

Electronic paramagnetic resonance (EPR)

As occurs with other similar compounds that exhibit strong antiferromagnetic couplings through two high-spin iron(III) centres,[97] we did not expect to obtain EPR signal for this compound. However, the X-band EPR spectral measurements carried out for μ-O-$[FeTCPP]_2$·16DMF at room temperature in solid state show an axially symmetric spectra with $g_\perp$ and $g_\parallel$ values close to 6 and 2 , respectively; unequivocal evidence of high spin Fe^{III} (S = 5/2) ions (Figure 7). The observed signal should therefore be caused by the monomeric species detected by magnetic measurements.

As observed in Figure 7, the parallel component exhibits a superhyperfine structure ($A_\parallel$ =17 Gauss) that is not habitual for this type of compounds. This superhyperfine structure can be explained by the interaction between the Fe^{III} electronic spin and the nuclear spins (I=1) of the four pyrrolic nitrogen atoms bonded to each Fe^{III} ion on the equatorial plane. This interaction should produce a nine-line structure. However, taking into account the ZFS effect confirmed for μ-O-$[FeTCPP]_2$·16DMF, this structure should be repeated at least in two different transitions within the S = 5/2 state. The fact that this superhyperfine structure has not been previously observed in similar compounds can be explained if considering that the magnetic matrix is very diluted for μ-O-$[FeTCPP]_2$·16DMF, due to the fact that 47% of the unit cell is occupied by DMF molecules. Therefore, the dilution of the magnetic matrix, induced by the porous nature of the compound, allows the unusual observance of electronic and nuclear spin interactions between different atoms.

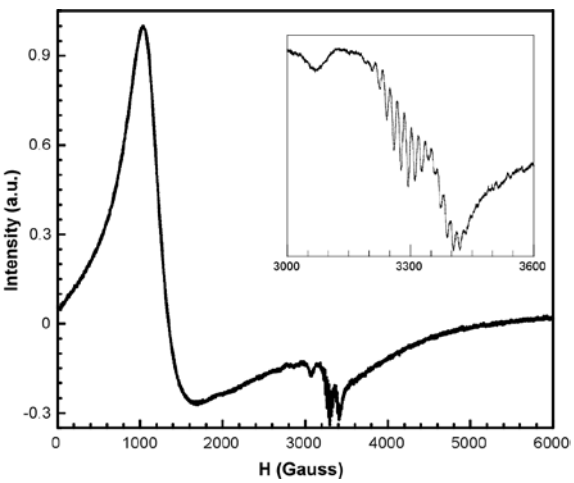

Fig. 7 X-band EPR spectrum for μ-O-$[FeTCPP]_2$·16DMF registered at room temperature.

Catalytic properties

Synthetic metalloporphyrins complexes have been largely used for a variety of catalytic transformations,[19] and a special emphasis has been placed on the single atom bridged diiron complexes as an emerging class of catalysts.[98] In this sense, μ-O-$[FeTCPP]_2$·16DMF exhibits two additional characteristics that make one think of its potential as a catalyst. Firstly, Fe^{III} centres are five-coordinated square pyramidal polyhedra. Secondly, the network is significantly accessible, with mobile DMF molecules located in the cavities. Therefore, virtually approaching to the metal ion by other molecules in dissolution seems to be easy. The above mentioned aspects were considered to proceed with the study of the catalytic properties of μ-O-$[FeTCPP]_2$·16DMF. Thus, the catalytic activity of μ-O-$[FeTCPP]_2$·16DMF was preliminarily tested towards oxidation of alcohols.

Oxidation of alcohols

The oxidation of alcohols is of great importance on organic synthesis and, in this sense, many iron porphyrins have been tested for this reaction.[46,99] As observed in many biological and biomimetic iron porphyrin models, in the presence of an oxidizing agent, Fe^{IV}-oxo complexes could be generated at the Fe^{III} sites[100] which could efficiently catalyze the oxidation of alcohol to the respective aldehydes. This iron(IV)-oxo unit has a Fe-O double character bond. Fe^{III} sites are regenerated when the oxidation takes place.[101]

The reaction conditions were firstly set using benzyl alcohol as model substrate. The reactions were carried out with TBHP as oxidizing agent in acetonitrile. Using a 5% of catalyst, 1.5 eq. of TBHP in 2 mL of solvent at 70 ºC a total conversion of 73% was obtained after 7 hours of reaction (Table 2). The effect of the oxidizing agent was studied using $PhI(OAc)_2$ (2 eq.), instead of TBHP, obtaining a 69 % conversion rate after 7 hours. Both the yield and the kinetic profile (Figure 8) of the reactions are very similar, therefore the oxidizing agent have no much influence in the catalytic activity of μ-O-$[FeTCPP]_2$·16DMF.

The substrate scope was studied with various alcohols, 1-phenylethanol, 1-hexanol and 1-octanol in TBHP (1.5 eq.). Figure 8 shows the kinetic profiles of the oxidation reactions. As observed, μ-O-$[FeTCPP]_2$·16DMF catalyses more effectively activated alcohols (benzyl alcohol and 1-phenylethanol) than lineal ones, because they present more steric hindrance.

The yield for activated alcoholic substrates lies within the habitual range for similar porphyrinic catalysts. However, comparison with data found in literature indicates that there is a significant reduction in the reaction time for μ-O-$[FeTCPP]_2$·16DMF; in fact, in some cases, the conversion is reached in half of the time.[101]

Table 2 Selective oxidation of several alcohols over μ-O-[FeTCPP]$_2$·16DMF catalyst.

	Substrate	Oxidant	Product	TON[a]	TOF (h^{-1})[b]
1	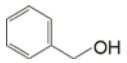	TBHP	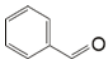	24	72
		$PhI(OAc)_2$		23	50
2	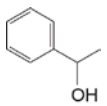	TBHP		25	91
3		TBHP		5	3
4		TBHP		3	3

[a]TON: Turnover number: mol subs.conv./mol cat,
[b]TOF: mol subst.conv./mol cat. h)

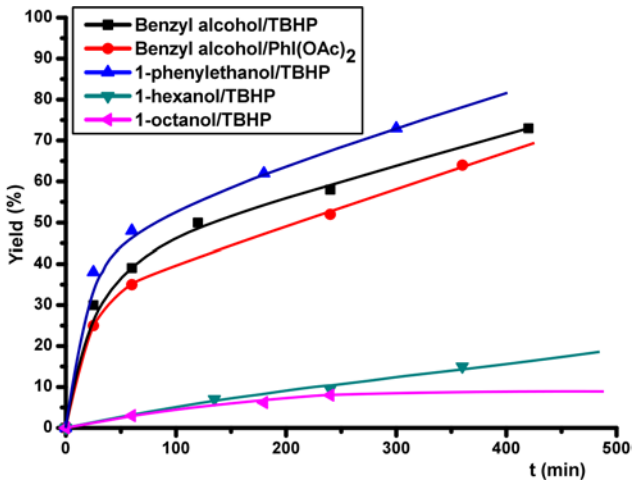

Fig. 8 Kinetic profiles for the alcohol oxidation reactions.

After the oxidation reactions, the solid catalyst was recovered by centrifugation, washed with acetonitrile and ethanol, and then characterised by IR spectroscopy. The IR spectra of the recovered catalyst for the tested oxidation reactions show that the structural units remain, in fact, the solid shows the same characteristic vibration modes of the original compound. As shown in Figure S6, ESI† the characteristic vibrations of the porphyrin macrocycle are present, including the Fe-TCPP and Fe-O-Fe vibrations at 1000 cm^{-1}, 870 cm^{-1} and 824 cm^{-1}.

Heterogeneity and recyclability tests

A heterogeneity test was carried out for the oxidation of benzyl alcohol over μ-oxo-FeTCPP sample. For rigorous proof of heterogeneity, the test[102] was carried out by filtering the catalyst from the reaction mixture at 70 ºC after 25 min, when a conversion rate of 34 % had been reached. The filtrate was allowed to react for up to 7 h. The reaction mixture and the filtrate were analysed after 7 h by GC-MS. No significant change in the conversion rate was found for the filtrate (Figure 9), meaning that the active species does not leach and the observed catalysis is truly heterogeneous in nature.

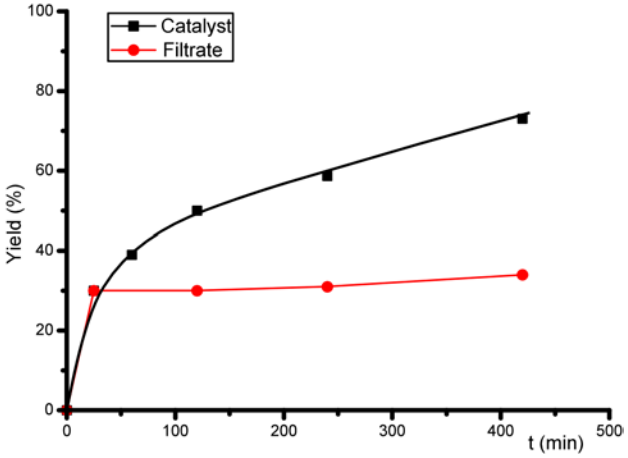

Fig. 9 Kinetic profile of oxidation of benzyl alcohol over μ-O-[FeTCPP]$_2$·16DMF and after hot filtering, with TBHP.

Reutilization is one of the greatest advantages of heterogeneous catalysts and can also provide useful information about the anchoring process and catalyst stability along the catalytic cycles. Thus, recycling tests were carried out over μ-O-[FeTCPP]$_2$·16DMF for the oxidation of benzyl alcohol with $PhI(OAc)_2$ and, as observed in Table 3, during the three cycles an increase of catalytic activity is observed. This could mean that the catalytic active species formed in the presence of the oxidant increases after the first run.

Table 3 Recyclability of compound μ-O-[FeTCPP]$_2$·16DMF for benzyl alcohol oxidation.

Cycles	C_T (4h)
1	58 %
2	77 %
3	98 %

C_T = Total conversion

Conclusions

FeTCPP metalloporphyrin cation has been used to produce a new solid based on unprecedented μ-oxo-FeTCPP dimers. The coordination network exhibits significant free volume, related to the unusual appearance of a superhyperfine EPR structure. Additionally, the accessibility to the network in the compound, along with the structural features of the dimers, is responsible for its catalytic properties. Those characteristics allow μ-O-[FeTCPP]$_2$ to be playing a double role, as a catalyst and as a synthon. Therefore, this is an innovative approach to achieve heterogeneous catalyst as an alternative to the anchoring of effective catalyst into solid frameworks. It is worth mentioning that the existence of an extended coordination network is not necessary to a stable and functional solid. Furthermore, the catalytic activity studies herein presented are a starting point for the application of these materials as heterogeneous catalysts in other reactions of interest in fine chemistry.

Acknowledgments

This work has been financially supported by the ‘‘Ministerio de

Economia y Competitividad" (MAT2013-42092-R, MAT2011-29020-C02-02), the ''Gobierno Vasco'' (Basque University System Research Groups, IT-630-13) and UPV/EHU (UFI 11/15) which we gratefully acknowledge. The technical and human support provided by SGIker is gratefully acknowledged. The authors thank Dr. Estibaliz Legarra (UPV/EHU) for the Mössbauer measurements. A. Fidalgo-Marijuan thanks to the UPV/EHU fellowships.

Notes and references

[a] *Departamento de Mineralogía y Petrología and* [b] *Departamento de Química Inorgánica, Facultad de Ciencia y Tecnología, Universidad del País Vasco (UPV/EHU), Apdo. 644, 48080 Bilbao, Spain, Fax: +34 946 013 500; Tel: +34 946 015 984; E-mail: arkaitz.fidalgo@ehu.es, gotzone.barandika@ehu.es, bego.bazan@ehu.es, karmele.urtiaga@ehu.es, edurne.serrano@ehu.es, luis.lezama@ehu.es, maribel.arriortua@ehu.es,*

[c] *Instituto de Ciencia de Materiales de Madrid-CSIC, Sor Juana Inés de la Cruz 3, Cantoblanco, 28049 Madrid, Spain, Fax: +34 913 720 623; Tel: +34 913 349 032; E-mail: marta.iglesias@icmm.csic.es*

[d] *BCMaterials Parque Tecnológico de Zamudio, Ibaizabal Bidea, Edificio 500-Planta 1, 48160, Derio, Spain*

† Electronic Supplementary Information (ESI) available: ORTEP detail of the structure, IR, Raman and UV/Vis spectra, thermogravimetry, IR of the catalysis residues, crystallographic data and CIF file. CCDC 981624. See DOI: 10.1039/b000000x/

1. K. K. Tanabe and S. M. Cohen, *Chem. Soc. Rev.*, 2011, **40**, 498-519.
2. J. R. Long and O. M. Yaghi, *Chem. Soc. Rev.*, 2009, **38**, 1213-1214.
3. S. R. Batten, N. R. Champness, X.-M. Chen, J. Garcia-Martinez, S. Kitagawa, L. Oehrstroem, M. O'Keeffe, M. P. Suh and J. Reedijk, *CrystEngComm*, 2012, **14**, 3001-3004.
4. M. Eddaoudi, J. Kim, N. Rosi, D. Vodak, J. Wachter, M. O'Keeffe and O. M. Yaghi, *Science*, 2002, **295**, 469-472.
5. P. Suh Myunghyun, J. Park Hye, K. Prasad Thazhe and D.-W. Lim, *Chem. Rev.*, 2012, **112**, 782-835.
6. C. Wang, T. Zhang and W. Lin, *Chem. Rev.*, 2012, **112**, 1084-1104.
7. O. R. Evans and W. Lin, *Acc. Chem. Res.*, 2002, **35**, 511-522.
8. W. Zhang and R.-G. Xiong, *Chem. Rev.*, 2012, **112**, 1163-1195.
9. T. C. Narayan, T. Miyakai, S. Seki and M. Dinca, *J. Am. Chem. Soc.*, 2012, **134**, 12932-12935.
10. M. Kurmoo, *Chem. Soc. Rev.*, 2009, **38**, 1353-1379.
11. Y. Cui, Y. Yue, G. Qian and B. Chen, *Chem. Rev.*, 2012, **112**, 1126-1162.
12. D. Liu, R. C. Huxford and W. Lin, *Angew. Chem., Int. Ed.*, 2011, **50**, 3696-3700.
13. E. Kreno Lauren, K. Leong, K. Farha Omar, M. Allendorf, P. Van Duyne Richard and T. Hupp Joseph, *Chem. Rev.*, 2012, **112**, 1105-1125.
14. P. Horcajada, T. Chalati, C. Serre, B. Gillet, C. Sebrie, T. Baati, J. F. Eubank, D. Heurtaux, P. Clayette, C. Kreuz, J.-S. Chang, Y. K. Hwang, V. Marsaud, P.-N. Bories, L. Cynober, S. Gil, G. Ferey, P. Couvreur and R. Gref, *Nat. Mater.*, 2010, **9**, 172-178.
15. L. Ma, J. M. Falkowski, C. Abney and W. Lin, *Nat. Chem.*, 2010, **2**, 838-846.
16. R. Fernandez de Luis, M. K. Urtiaga, J. L. Mesa, E. S. Larrea, M. Iglesias, T. Rojo and M. I. Arriortua, *Inorg. Chem.*, 2013, **52**, 2615-2626.
17. J. Orive, E. S. Larrea, R. Fernandez de Luis, M. Iglesias, J. L. Mesa, T. Rojo and M. I. Arriortua, *Dalton Trans.*, 2013, **42**, 4500-4512.
18. I. Beletskaya, V. S. Tyurin, A. Y. Tsivadze, R. Guilard and C. Stern, *Chem. Rev.*, 2009, **109**, 1659-1713.
19. B. Meunier, *Chem. Rev.*, 1992, **92**, 1411-1456.
20. C. M. Lemon, D. K. Dogutan and D. G. Nocera, *Handbook of Porphyrin Science*, World Scientific Publishing Co. Pte. Ltd., Singapore, Singapore, 2012.
21. J. T. Hupp, *Nat. Chem.*, 2010, **2**, 432-433.
22. M. M. Q. Simoes, C. M. B. Neves, S. M. G. Pires, M. G. P. M. S. Neves and J. A. S. Cavaleiro, *Pure Appl. Chem.*, 2013, **85**, 1671-1681.
23. S. Chatterjee, K. Sengupta, S. Samanta, P. K. Das and A. Dey, *Inorg. Chem.*, 2013, **52**, 9897-9907.
24. S. Zakavi, F. Heidarizadi and S. Rayati, *Inorg. Chem. Commun.*, 2011, **14**, 1010-1013.
25. E. V. Kudrik, P. Afanasiev, L. X. Alvarez, P. Dubourdeaux, M. Clemancey, J.-M. Latour, G. Blondin, D. Bouchu, F. Albrieux, S. E. Nefedov and A. B. Sorokin, *Nat. Chem.*, 2012, **4**, 1024-1029.
26. G. Ricciardi, A. Rosa, J. Baerends Evert and A. J. Van Gisbergen Stan, *J Am Chem Soc*, 2002, **124**, 12319-12334.
27. R. A. Sheldon, *Metalloporphyrins in Catalytic Oxidations*, Marcel Dekker, Inc., New York, 1994.
28. R. Patra, S. Bhowmik, S. K. Ghosh and S. P. Rath, *Eur. J. Inorg. Chem.*, 2009, 654-655.
29. P. D. Harvey, C. Stern, C. P. Gros and R. Guilard, *Coord. Chem. Rev.*, 2007, **251**, 401-428.
30. X. D. Jiao, J. W. Huang, L. N. Ji, B. S. Luo and L. R. Chen, *J. Inorg. Biochem.*, 1997, **65**, 229-233.
31. H. Yang, J. Li, L. Wang, W. Dai, Y. Lv and S. Gao, *Catal. Commun.*, 2013, **35**, 101-104.
32. R. E. Hansen and S. Das, *Energy Environ. Sci.*, 2014, **7**, 317-322.
33. C. L. Whittington, L. Wojtas and R. W. Larsen, *Inorg. Chem.*, 2014, **53**, 160-166.
34. C. Wang, Z. Xie, E. deKrafft Kathryn and W. Lin, *J. Am. Chem. Soc.*, 2011, **133**, 13445-13454.
35. A. M. Rasero-Almansa, A. Corma, M. Iglesias and F. Sanchez, *ChemCatChem*, 2013, **5**, 3092-3100.
36. M. Pintado-Sierra, A. M. Rasero-Almansa, A. Corma, M. Iglesias and F. Sanchez, *J. Catal.*, 2013, **299**, 137-145.
37. D. Feng, W.-C. Chung, Z. Wei, Z.-Y. Gu, H.-L. Jiang, Y.-P. Chen, D. J. Darensbourg and H.-C. Zhou, *J. Am. Chem. Soc.*, 2013, **135**, 17105-17110.
38. Z. Zhang, L. Zhang, L. Wojtas, P. Nugent, M. Eddaoudi and M. J. Zaworotko, *J. Am. Chem. Soc.*, 2012, **134**, 924-927.
39. Z. Zhang, L. Zhang, L. Wojtas, M. Eddaoudi and M. J. Zaworotko, *J. Am. Chem. Soc.*, 2012, **134**, 928-933.
40. C. Zou, Z. Zhang, X. Xu, Q. Gong, J. Li and C.-D. Wu, *J. Am. Chem. Soc.*, 2012, **134**, 87-90.
41. M. Jahan, Q. Bao and K. P. Loh, *J. Am. Chem. Soc.*, 2012, **134**, 6707-6713.
42. X.-L. Yang, M.-H. Xie, C. Zou, Y. He, B. Chen, M. O'Keeffe and C.-D. Wu, *J. Am. Chem. Soc.*, 2012, **134**, 10638-10645.
43. O. K. Farha, A. M. Shultz, A. A. Sarjeant, S. T. Nguyen and J. T. Hupp, *J. Am. Chem. Soc.*, 2011, **133**, 5652-5655.
44. L. Chen, Y. Yang and D. Jiang, *J. Am. Chem. Soc.*, 2010, **132**, 9138-9143.
45. A. M. Shultz, O. K. Farha, J. T. Hupp and S. T. Nguyen, *J. Am. Chem. Soc.*, 2009, **131**, 4204-4205.
46. C. Zou, T. Zhang, M.-H. Xie, L. Yan, G.-Q. Kong, X.-L. Yang, A. Ma and C.-D. Wu, *Inorg. Chem.*, 2013, **52**, 3620-3626.
47. M.-H. Xie, X.-L. Yang, Y. He, J. Zhang, B. Chen and C.-D. Wu, *Chem. - Eur. J.*, 2013, **19**, 14316-14321.
48. M.-H. Xie, X.-L. Yang, C. Zou and C.-D. Wu, *Inorg. Chem.*, 2011, **50**, 5318-5320.
49. M. Zhao, S. Ou and C. D. Wu, *Acc Chem Res*, 2014, **47**, 1199-1207.
50. A. Fidalgo-Marijuan, G. Barandika, B. Bazan, M.-K. Urtiaga and M.-I. Arriortua, *Polyhedron*, 2011, **30**, 2711-2716.
51. A. Fidalgo-Marijuan, G. Barandika, B. Bazan, M. K. Urtiaga and M. I. Arriortua, *Crystengcomm*, 2013, **15**, 4181-4188.
52. A. Fidalgo-Marijuan, G. Barandika, B. Bazan, M. K. Urtiaga, L. Lezama and M. I. Arriortua, *Inorg. Chem.*, 2013, **52**, 8074-8081.
53. A. Fidalgo-Marijuan, UPV/EHU, Leioa, Spain, 2014. Ph. D. Thesis.
54. W. Chen and S. Fukuzumi, *Eur. J. Inorg. Chem.*, 2009, 5494-5505.
55. P. M. Barron, H.-T. Son, C. Hu and W. Choe, *Cryst. Growth Des.*, 2009, **9**, 1960-1965.
56. S. H. Strauss, M. J. Pawlik, J. Skowyra, J. R. Kennedy, O. P. Anderson, K. Spartalian and J. L. Dye, *Inorg. Chem.*, 1987, **26**, 724-730.
57. D. V. Konarev, S. S. Khasanov and R. N. Lyubovskaya, *J. Porphyrins Phthalocyanines*, 2010, **14**, 293-297.

58. M. Li, M. Shang, H. F. Duval and W. R. Scheidt, *Acta Crystallogr., Sect. C Cryst. Struct. Commun.*, 2000, **C56**, 1206-1207.
59. K. M. Kadish, M. Autret, Z. Ou, P. Tagliatesta, T. Boschi and V. Fares, *Inorg. Chem.*, 1997, **36**, 204-207.
60. D. R. Evans, R. S. Mathur, K. Heerwegh, C. A. Reed and Z. Xie, *Angew. Chem.*, 1997, **36**, 1335-1337.
61. T. J. Bartczak, L. Latos-Grazynski and A. Wyslouch, *Inorg. Chim. Acta*, 1990, **171**, 205-212.
62. A. L. Litvinov, D. V. Konarev, A. Y. Kovalevsky, A. N. Lapshin, E. I. Yudanova, N. V. Drichko, P. Coppens and R. N. Lyubovskaya, *Eur. J. Inorg. Chem.*, 2003, 3914-3917.
63. A. B. Hoffman, D. M. Collins, V. W. Day, E. B. Fleischer, T. S. Srivastava and J. L. Hoard, *J. Am. Chem. Soc.*, 1972, **94**, 3620-3626.
64. K. L. Lay, J. W. Buchler, J. E. Kenny and W. R. Scheidt, *Inorg. Chim. Acta*, 1986, **123**, 91-97.
65. W. R. Scheidt, B. Cheng, M. K. Safo, F. Cukiernik, J. C. Marchon and P. G. Debrunner, *J. Am. Chem. Soc.*, 1992, **114**, 4420-4421.
66. Y. Deng, C. J. Chang and D. G. Nocera, *J. Am. Chem. Soc.*, 2000, **122**, 410-411.
67. S. K. Ghosh, R. Patra and S. P. Rath, *Inorg. Chim. Acta*, 2010, **363**, 2791-2799.
68. S. K. Ghosh and S. P. Rath, *J. Am. Chem. Soc.*, 2010, **132**, 17983-17985.
69. C. Da Silva, L. Bonomo, E. Solari, R. Scopelliti, C. Floriani and N. Re, *Chem. - Eur. J.*, 2000, **6**, 4518-4531.
70. C. J. Chang, Z.-H. Loh, C. Shi, F. C. Anson and D. G. Nocera, *J. Am. Chem. Soc.*, 2004, **126**, 10013-10020.
71. S. K. Ghosh, R. Patra and S. P. Rath, *Inorg. Chem.*, 2008, **47**, 10196-10198.
72. A. L. Balch, B. C. Noll, M. M. Olmstead and S. L. Phillips, *Inorg. Chem.*, 1996, **35**, 6495-6506.
73. H. M. Lee, M. M. Olmstead, G. G. Gross and A. L. Balch, *Cryst. Growth Des.*, 2003, **3**, 691-697.
74. B. Cheng, J. D. Hobbs, P. G. Debrunner, J. Erlebacher, J. A. Shelnutt and W. R. Scheidt, *Inorg. Chem.*, 1995, **34**, 102-110.
75. W. P. Schaefer, P. E. Ellis, J. E. Lyons and S. N. Shaikh, *Acta Crystallogr., Sect. C Cryst. Struct. Commun.*, 1995, **C51**, 2252-2255.
76. S. Bhowmik, S. K. Ghosh, S. Layek, H. C. Verma and S. P. Rath, *Chem. - Eur. J.*, 2012, **18**, 13025-13037.
77. M. Khorasani-Motlagh, M. Noroozifar, J. Saffari and B. O. Patrick, *J. Struct. Chem.*, 2012, **53**, 593-597.
78. W. Yinghua, *J. Appl. Crystallogr.*, 1987, **20**, 258-259.
79. , Agilent Technologies UK Ltd.: Oxford, U. K., 2012.
80. L. Palatinus and G. Chapuis, *J. Appl. Crystallogr.*, 2007, **40**, 786-790.
81. G. M. Sheldrick, *Acta Crystallogr., Sect. A Found. Crystallogr.*, 2008, **A64**, 112-122.
82. O. V. Dolomanov, L. J. Bourhis, R. J. Gildea, J. A. K. Howard and H. Puschmann, *J. Appl. Crystallogr.*, 2009, **42**, 339-341.
83. A.-R. Li, H.-H. Wei and L.-L. Gang, *Inorg. Chim. Acta*, 1999, **290**, 51-56.
84. A. Gold, K. Jayaraj, P. Doppelt, J. Fischer and R. Weiss, *Inorg. Chim. Acta*, 1988, **150**, 177-181.
85. K. D. Karlin, A. Nanthakumar, S. Fox, N. N. Murthy, N. Ravi, B. H. Huynh, R. D. Orosz and E. P. Day, *J. Am. Chem. Soc.*, 1994, **116**, 4753-4763.
86. M. R. Johnson, W. K. Seok, W. Ma, C. Slebodnick, K. M. Wilcoxen and J. A. Ibers, *J. Org. Chem.*, 1996, **61**, 3298-3303.
87. M. Suzuki, K. Tsuge, Y. Sasaki and T. Imamura, *Chem. Lett.*, 2003, **32**, 564-565.
88. A. L. Spek, Utrech University, Utrecht, The Netherlands, 1998.
89. W. Jentzen, X.-Z. Song and J. A. Shelnutt, *J. Phys. Chem. B*, 1997, **101**, 1684-1699.
90. W. Jentzen, J.-G. Ma and J. A. Shelnutt, *Biophys. J.*, 1998, **74**, 753-763.
91. R. Weiss, A. Gold and J. Terner, *Chem. Rev.*, 2006, **106**, 2550-2579.
92. C. Ercolani, M. Gardini, F. Monacelli, G. Pennesi and G. Rossi, *Inorg. Chem.*, 1983, **22**, 2584-2589.
93. J. M. Burke, J. R. Kincaid and T. G. Spiro, *J. Am. Chem. Soc.*, 1978, **100**, 6077-6083.
94. F. L. Benedito, S. Nakagaki, A. A. Saczk, P. G. Peralta-Zamora and C. M. M. Costa, *Appl. Catal., A*, 2003, **250**, 1-11.
95. L. W. Finger and R. M. Hazen, *J. Appl. Phys.*, 1980, **51**, 5362-5367.
96. R. A. Brand, J. Lauer and D. M. Herlach, *J. Phys. F: Met. Phys.*, 1983, **13**, 675-683.
97. S. K. Ghosh, R. Patra and S. P. Rath, *Inorg. Chem.*, 2010, **49**, 3449-3460.
98. A. B. Sorokin, *Chem. Rev.*, 2013, **113**, 8152-8191.
99. G. S. Machado, O. Jose de Lima, K. J. Ciuffi, F. Wypych and S. Nakagaki, *Catal. Sci. Technol.*, 2013, **3**, 1094-1101.
100. W. Nam, *Acc. Chem. Res.*, 2007, **40**, 522-531.
101. A. Modak, J. Mondal and A. Bhaumik, *Appl. Catal., A*, 2013, **459**, 41-51.
102. R. A. Sheldon, M. Wallau, I. W. C. E. Arends and U. Schuchardt, *Acc. Chem. Res.*, 1998, **31**, 485-493.